J. Fluid Mech. (1999), *vol.* 384, *pp.* 183–206. Printed in the United Kingdom

Drag and lift forces on a rotating sphere in a linear shear flow

By RYOICHI KUROSE† AND SATORU KOMORI
Department of Mechanical Engineering, Kyoto University, Kyoto 606-8501, Japan

(Received 20 August 1997 and in revised form 6 November 1998)

The drag and lift forces acting on a rotating rigid sphere in a homogeneous linear shear flow are numerically studied by means of a three-dimensional numerical simulation. The effects of both the fluid shear and rotational speed of the sphere on the drag and lift forces are estimated for particle Reynolds numbers of $1 \leqslant Re_p \leqslant 500$.

The results show that the drag forces both on a stationary sphere in a linear shear flow and on a rotating sphere in a uniform unsheared flow increase with increasing the fluid shear and rotational speed. The lift force on a stationary sphere in a linear shear flow acts from the low-fluid-velocity side to the high-fluid-velocity side for low particle Reynolds numbers of $Re_p < 60$, whereas it acts from the high-velocity side to the low-velocity side for high particle Reynolds numbers of $Re_p > 60$. The change of the direction of the lift force can be explained well by considering the contributions of pressure and viscous forces to the total lift in terms of flow separation. The predicted direction of the lift force for high particle Reynolds numbers is also examined through a visualization experiment of an iron particle falling in a linear shear flow of a glycerin solution. On the other hand, the lift force on a rotating sphere in a uniform unsheared flow acts in the same direction independent of particle Reynolds numbers. Approximate expressions for the drag and lift coefficients for a rotating sphere in a linear shear flow are proposed over the wide range of $1 \leqslant Re_p \leqslant 500$.

1. Introduction

The motion of particles in turbulence is often seen in air and water flows related to significant environmental problems such as desertification and air pollution, and also occurs in many industrial processes associated with particle transport. It is, therefore, of great practical interest to investigate particle motion both in settling environmental problems and in designing industrial equipment. In particular, particle motion in a turbulent boundary layer is influenced by both the fluid shear and particle rotation which will be induced by the fluid shear and collisions with a solid wall. Therefore it is also of importance to investigate the effects of the fluid shear and particle rotation on the fluid forces acting on a particle by means of experiments and numerical simulations.

Rubinow & Keller (1961) and Saffman (1965) showed that a lift force acts on a rotating sphere in a linear unbounded shear flow by using matched asymptotic expansions. In their analyses, the particle Reynolds number $Re_p(= 2aU_c/\nu)$ was assumed to be much less than unity. Here $2a$ is the diameter of the sphere, U_c is the fluid velocity on the streamline through the centre of the sphere, and ν is the

† Present address: Yokosuka Research Laboratory, Central Research Institute of Electric Power Industry (CRIEPI), Yokosuka, Kanagawa 240-0196, Japan.

kinematic viscosity. Saffman's expression for the lift force on a sphere derived by higher-order approximations is given by

$$F_L = 6.46\nu\rho_f a^2 U_c(|\alpha|/\nu)^{1/2} - \tfrac{11}{8}\rho_f U_c \alpha a^3 + \pi\rho_f U_c \Omega a^3, \tag{1.1}$$

where ρ_f is the fluid density, α is the fluid shear rate of the mean flow, and Ω is the rotational angular speed of the sphere. The first and second terms on the right-hand side are due to the fluid shear, and the third term takes account of the effect of the rotation of the sphere. The sign of the first term is positive for positive α, and it is negative for negative α. The lift force on a stationary ($\Omega = 0$) sphere in a linear shear flow always acts towards the higher-fluid-velocity side, and a rotating sphere with clockwise rotation in a uniform unsheared flow ($\alpha = 0$) generates upward lift. Saffman (1965) has mentioned that unless the rotational speed of a freely rotating sphere with a small particle Reynolds number is much greater than the shear rate, the lift force due to the rotation is less by an order of magnitude than that due to the shear. Therefore, the second and third terms on the right-hand side in (1.1) were neglected for low particle Reynolds numbers in many previous studies.

However, expression (1.1) cannot be applied to large particle Reynolds numbers of $Re_p \gg 1$. To estimate the lift force acting on a stationary sphere in a linear shear flow with a higher particle Reynolds number, Hall (1988) and Mollinger & Nieuwstadt (1996) tried to measure the lift force acting on a particle in a wind tunnel, and Dandy & Dwyer (1990) carried out three-dimensional numerical simulations for a linear shear flow around a stationary sphere at $Re_p = 0.1$–100. By using the results of Saffman (1965) and Dandy & Dwyer (1990), Mei (1992) proposed an approximate expression for the lift force for finite Re_p. On the other hand, Jordan & Fromm (1972) numerically estimated the lift force acting on a cylinder with a higher particle Reynolds number of $Re_p = 400$, and showed a very interesting result: the lift force on the cylinder surface acted in the opposite direction to that found in other studies (e.g. Saffman 1965; Dandy & Dwyer 1990). Although the difference of the lift force direction may be due to the difference in the shape of a three-dimensional sphere and a two-dimensional cylinder, this has not been elucidated. Therefore, it is of great interest to numerically estimate the lift force acting on a sphere for high particle Reynolds numbers of $Re_p > 100$.

To investigate the effect of the rotation of a sphere, the drag and lift forces have been measured for very high particle Reynolds numbers of $Re_p = 10^3$–10^6 (e.g. Barkla & Auchterlonie 1971; Rabindra 1985). Tsuji, Morikawa & Mizuno (1985) measured the lift force on a rotating sphere for $550 \leqslant Re_p \leqslant 1600$. Salem & Oesterle (1995) numerically investigated the interaction between the fluid shear and rotation on the lift force acting on a rotating sphere for $Re_p \leqslant 10$ in a linear shear flow. However, the lift force for arbitrary values of the fluid shear rate, rotational speed and particle Reynolds number could not be estimated because of the lack of data.

On the other hand, the variation of the drag force with the fluid shear rate was investigated analytically by Harper & Chang (1968) for a sphere with $Re_p \ll 1$ and numerically by Dandy & Dwyer (1990) for a sphere with $1 \leqslant Re_p \leqslant 100$. However the effect of the rotation on the drag force was not clarified.

The purpose of this study is to investigate the effects of the fluid shear and rotation on the drag and lift forces acting on a rotating sphere in a linear shear flow by means of a three-dimensional numerical simulation. The computations were carried out for $1 \leqslant Re_p \leqslant 500$. The effects of both fluid shear and rotation were clarified through the numerical predictions for three cases: a linear shear flow around a stationary sphere, a uniform unsheared flow around a rotating sphere, and a linear shear flow

around a rotating sphere. Furthermore, approximate expressions for the drag and lift coefficients applicable to arbitrary shear rate and rotational speed were derived from the numerical results. In addition to the numerical simulation, a visualization experiment on a falling iron particle was carried out in a linear shear flow of a glycerin solution to examine the predicted direction of the lift force acting on a stationary sphere in a linear shear flow with a high particle Reynolds number.

2. Numerical simulation

The flow geometry and coordinate system for computations are shown in figure 1. The imposed flow is a linear shear flow around a rotating sphere. The three-dimensional Navier–Stokes (N–S) equations were directly solved using a finite difference scheme based on the marker-and-cell (MAC) method and cylindrical coordinates were used (figure 2). The numerical procedure used here was essentially the same as that used by Hanazaki (1988) except for the presence of the fluid shear and boundary conditions. The dimensionless pressure–Poisson (P–P) equation was derived by taking divergence of the N–S equations:

$$\nabla^2 p = \frac{D}{\Delta t} - \nabla \cdot [(\boldsymbol{V} \cdot \nabla)\boldsymbol{V}] + \frac{2}{Re_p}\nabla^2 D, \tag{2.1}$$

and the dimensionless N–S equations are given by

$$\frac{\partial U}{\partial t} + (\boldsymbol{V} \cdot \nabla)U = -\frac{\partial p}{\partial x} + \frac{2}{Re_p}\nabla^2 U, \tag{2.2}$$

$$\frac{\partial V}{\partial t} + (\boldsymbol{V} \cdot \nabla)V - \frac{V^2}{r} = -\frac{\partial p}{\partial r} + \frac{2}{Re_p}\left(\nabla^2 V - \frac{V}{r^2} - \frac{2}{r^2}\frac{\partial V}{\partial \theta}\right), \tag{2.3}$$

$$\frac{\partial W}{\partial t} + (\boldsymbol{V} \cdot \nabla)W + \frac{VW}{r} = -\frac{1}{r}\frac{\partial p}{\partial \theta} + \frac{2}{Re_p}\left(\nabla^2 W - \frac{W}{r^2} + \frac{2}{r^2}\frac{\partial W}{\partial \theta}\right). \tag{2.4}$$

The dimensionless P–P equation and N–S equations were solved alternately. Here D, V, ∇^2 and Re_p are defined by

$$D = \nabla \cdot \boldsymbol{V}, \tag{2.5}$$

$$\boldsymbol{V} = (V_x, V_r, V_\theta) = (U, V, W), \tag{2.6}$$

$$\nabla^2 = \frac{\partial^2}{\partial x^2} + \frac{1}{r}\frac{\partial}{\partial r}\left(r\frac{\partial}{\partial r}\right) + \frac{1}{r^2}\frac{\partial^2}{\partial \theta^2}, \tag{2.7}$$

$$Re_p = \frac{2aU_c}{\nu}, \tag{2.8}$$

where a is the radius of the sphere, ν is the kinematic viscosity, and U_c is the mean velocity of the fluid on the streamline through the centre of the sphere.

The boundary condition of the velocity upstream of a sphere is given in dimensionless form by

$$U = 1 + \alpha^* y, \tag{2.9}$$

and the boundary condition on the outer boundary, except upstream, is

$$\frac{\partial \boldsymbol{V}}{\partial x} = 0. \tag{2.10}$$

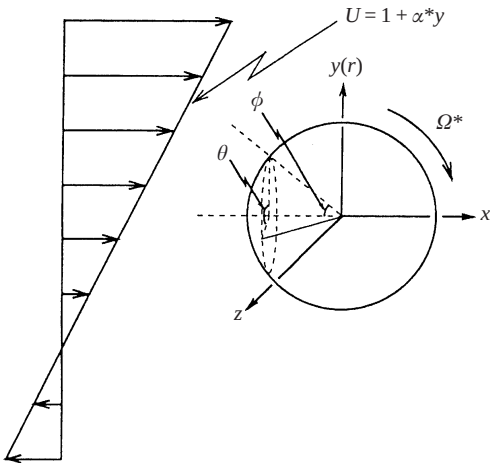

FIGURE 1. Coordinate system for a rotating sphere in a linear shear flow.

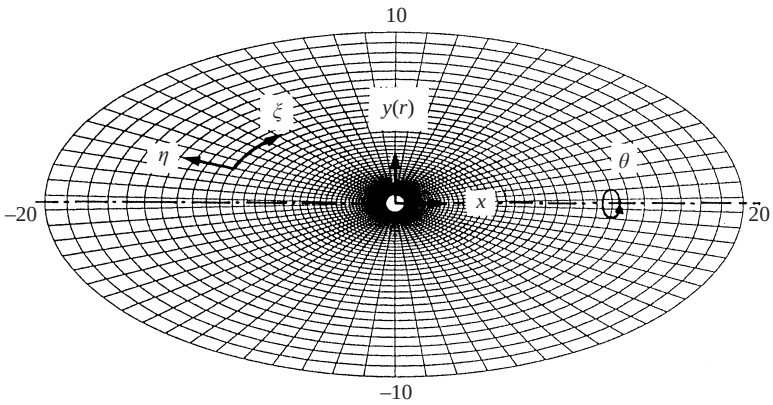

FIGURE 2. Side view of numerical grids on the centreplane ($z = 0$).

Here α^* is the dimensionless shear rate of the fluid:

$$\alpha^* = \frac{a}{U_c}\frac{\partial U}{\partial y}. \tag{2.11}$$

On the surface of a rotating sphere with an angular speed of Ω, the three components of the fluid velocity are given by

$$U = \frac{a\Omega\cos\theta\sin\phi}{U_c} = \Omega^*\cos\theta\sin\phi, \tag{2.12}$$

$$V = \frac{a\Omega\cos\theta\cos\phi}{U_c} = \Omega^*\cos\theta\cos\phi, \tag{2.13}$$

$$W = 0, \tag{2.14}$$

where Ω^* is the dimensionless rotational angular speed:

$$\Omega^* = \frac{a}{U_c}\Omega. \tag{2.15}$$

The computations were performed for particle Reynolds numbers of $1 \leqslant Re_p \leqslant 500$ ($Re_p = 1$, 2, 5, 10, 20, 50, 100, 200, 300, 400 and 500), shear rates of $0 \leqslant \alpha^* \leqslant 0.4$

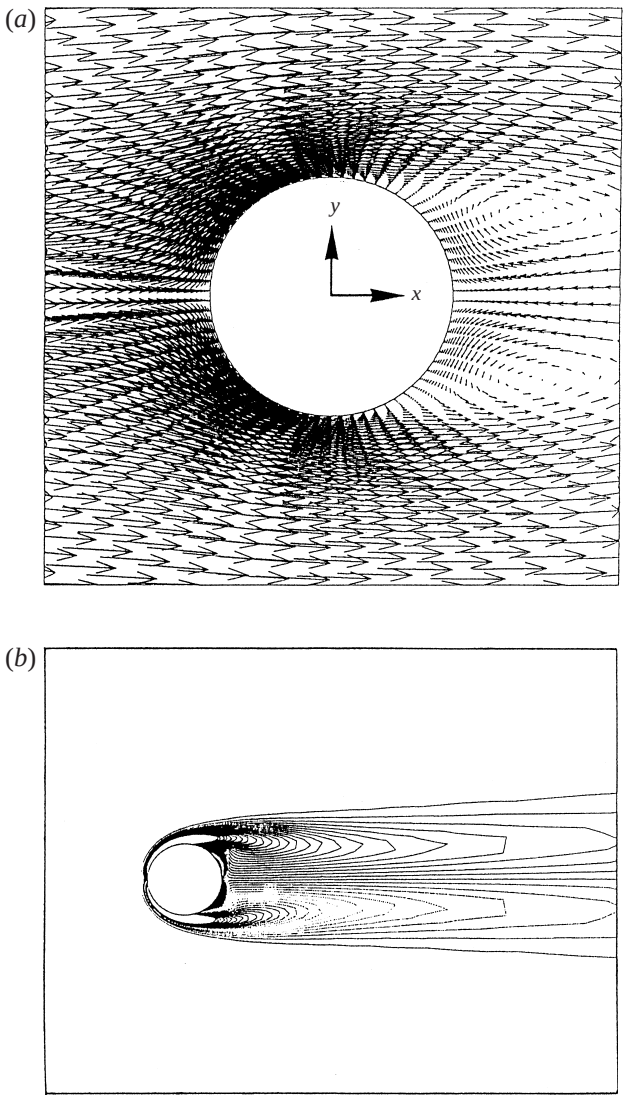

FIGURE 3. Velocity and vorticity fields around a stationary sphere in a uniform unsheared flow on the centreplane ($z = 0$) for $Re_p = 200$: (*a*) velocity field; (*b*) vorticity field.

($\alpha^* = 0$, 0.1, 0.2, 0.3 and 0.4), and angular speeds of $0 \leqslant \Omega^* \leqslant 0.25$ ($\Omega^* = 0$, 0.063, 0.16 and 0.25). In addition, the lift forces on a stationary sphere with $Re_p = 0.5$ and 3 were computed for $\alpha^* = 0$, 0.1 and 0.4 ($\Omega^* = 0$) to compare with the values obtained from the previous approximate expressions of Saffman (1965), McLaughlin (1991) and Mei (1992).

The drag and lift forces are the components of the fluid force acting on a sphere in the x- and y-directions, F_D and F_L, and they can be given by the sum of the pressure and viscous force contributions:

$$F_D = F_{D,p} + F_{D,f} = -\int_S p\boldsymbol{e}_x \cdot \boldsymbol{n}\,\mathrm{d}S + \int_S \boldsymbol{n}\cdot\boldsymbol{\tau}\cdot\boldsymbol{e}_x\,\mathrm{d}S, \tag{2.16}$$

$$F_L = F_{L,p} + F_{L,f} = -\int_S p\boldsymbol{e}_y \cdot \boldsymbol{n}\,\mathrm{d}S + \int_S \boldsymbol{n}\cdot\boldsymbol{\tau}\cdot\boldsymbol{e}_y\,\mathrm{d}S, \tag{2.17}$$

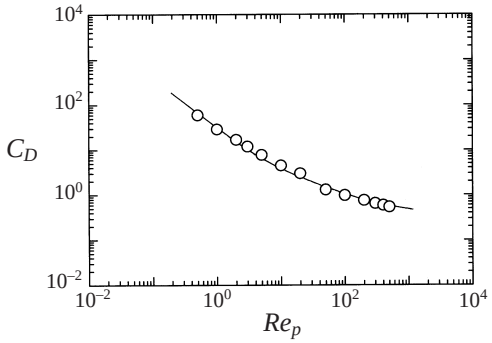

FIGURE 4. Comparison of the drag coefficient C_D for a stationary sphere in a uniform unsheared flow: ○, this study; ——, Morsi & Alexander (1972).

where τ is the viscous stress tensor. The drag and lift coefficients are defined by

$$C_D = \frac{F_D}{\frac{1}{2}\rho_f U_c^2 \pi a^2}, \tag{2.18}$$

$$C_L = \frac{F_L}{\frac{1}{2}\rho_f U_c^2 \pi a^2}, \tag{2.19}$$

where ρ_f is the fluid density.

By using a grid generation method developed by Thames *et al.* (1977), the grid points were concentrated near the sphere in the (x, r)-plane. The maximum sizes of the computational domain were 20 and 10 radii in the x- and r-directions, respectively. The (x, r, θ)-coordinate system was transformed to the (η, ξ, θ)-coordinate system with an equally grid spacing. The details of the coordinate system are described in Hanazaki (1988). The grid points used in this study were $35 \times 61 \times 48$ in the ξ-, η- and $\theta (0 \leqslant \theta \leqslant 2\pi)$ directions. To calculate the flow around a sphere accurately, several mesh points are required in the boundary layer. By using the above grid generation, ten or more the mesh points existed in the depth of the boundary layer which can be estimated as $1/Re_p^{1/2}$. The transformed governing equations were discretized to construct the finite difference formulation. The nonlinear terms in the N–S equations were approximated by a third-order scheme of Kawamura & Kuwahara (1984), and the other spatial derivatives were approximated by a second-order central difference scheme. Computations were repeated with a dimensionless time step of $\Delta t = 0.01$ until almost steady state was attained. However, oscillation of the lift force acting on a sphere with a high particle Reynolds number ($Re_p \geqslant 300$) was generated by the wake due to the flow separation behind the sphere, and therefore lift force was found by taking the time-averaged value over 30000 time steps (including several decades of the oscillation) during a quasi-steady state. The CPU time required for each case was about 3000 s on a NEC SX-3 super computer of the Center for the Global Environmental Research, National Institute for Environmental Studies.

3. Results and discussion

3.1. *Drag and lift on a stationary sphere*

Figure 3 shows the velocity and vorticity fields around a stationary sphere in a uniform unsheared flow ($Re_p = 200$, $\alpha^* = 0$, $\Omega^* = 0$) on the centreplane ($z = 0$). It is found

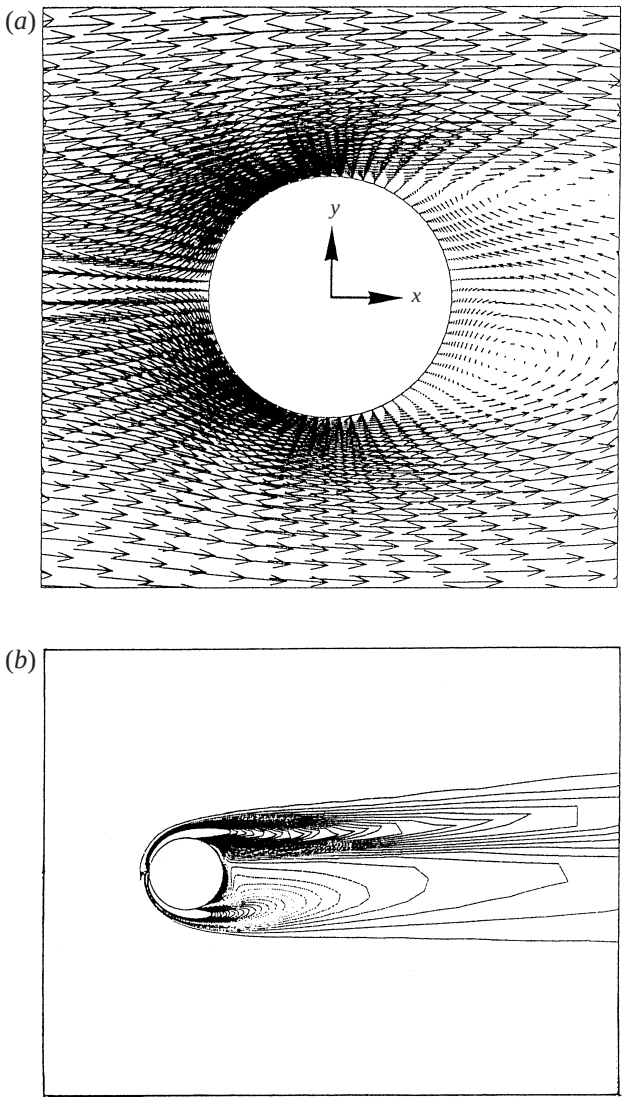

FIGURE 5. Velocity and vorticity fields around a stationary sphere in a linear shear flow on the centreplane ($z = 0$) for $Re_p = 200$ and $\alpha^* = 0.2$: (*a*) velocity field; (*b*) vorticity field.

that flow separations appear behind the sphere on both its upper and lower sides, and that symmetry exists with regard to the x-axis. Also, the points of flow separation (where tangential viscous stress is zero on the surface) tended to gradually move upstream with increasing Re_p. Figure 4 shows the variation of the drag coefficient C_D with the particle Reynolds number Re_p ($0.5 \leqslant Re_p \leqslant 500$), together with the results from Morsi & Alexander (1972), who proposed an expression C_D as a function of Re_p over a wide range of $Re_p < 50000$. The present C_D is in good agreement with their expression. On the other hand, although the time-averaged lift force was zero in an unsheared flow, remarkable oscillation of the instantaneous lift force occurred for the high Reynolds number of $Re_p \geqslant 300$. The Strouhal numbers based on the vortex shedding frequency f ($St = 2af/U_c$) were 0.128, 0.138 and 0.170 for $Re_p = 300$, 400 and 500, respectively. St was obtained using the time history of the lift coefficient

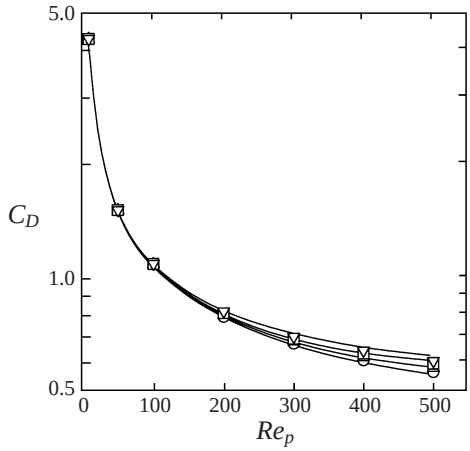

FIGURE 6. Drag coefficient C_D for a stationary sphere in a linear shear flow: ○, $\alpha^* = 0$; △, $\alpha^* = 0.1$; □, $\alpha^* = 0.2$; ▽, $\alpha^* = 0.4$.

C_L. Sakamoto & Haniu (1995) estimated St of the vortex shedding from a sphere in unsheared and shear flows in a water channel by means of flow visualization and velocity measurement ($200 \leqslant Re_p \leqslant 3000$). The present values of St are quantitatively in good agreement with the Sakamoto & Haniu's (1995) results.

In order to clarify the effects of the fluid shear on the drag and lift, the drag and lift coefficients were calculated for a stationary sphere in a linear shear flow ($0.5 \leqslant Re_p \leqslant 500$, $0 \leqslant \alpha^* \leqslant 0.4$ and $\Omega^* = 0$). Figure 5 shows the velocity and vorticity fields for this case ($Re_p = 200$, $\alpha^* = 0.2$) on the centreplane ($z = 0$). It is clearly illustrated that the wakes due to flow separation on the upper and lower sides behind the sphere are not symmetric with respect to the x-axis in a uniform unsheared flow. The drag coefficient C_D is plotted as a function of Re_p against the dimensionless shear rate α^* in figure 6. The value of C_D rapidly decreases with increasing Re_p. However, C_D increases with increasing α^* for a fixed value of Re_p, and the dependence of C_D on α^* is more obvious for higher Re_p. The difference in C_D between unsheared and sheared cases reaches about 10% at $Re_p = 500$ and $\alpha^* = 0.4$. The trend of C_D with α^* is similar to that of Dandy & Dwyer (1990).

To estimate the lift force on a sphere in a shear flow, Saffman (1965) analytically derived the expression (1.1) for a rotating sphere in a linear shear flow by using the following assumptions:

$$Re_p \ll 1, \tag{3.1}$$

$$Re_\Omega \left(= \frac{\Omega(2a)^2}{\nu} \right) \ll 1, \tag{3.2}$$

$$Re_\alpha \left(= \frac{\alpha(2a)^2}{\nu} \right) \ll 1, \tag{3.3}$$

$$\epsilon \left(= \frac{Re_\alpha^{1/2}}{Re_p} = 1.414 \left(\frac{\alpha^*}{Re_p} \right)^{1/2} \right) \gg 1. \tag{3.4}$$

From equation (1.1), we can derive the lift coefficient:

$$C_L = 5.816 \left(\frac{|\alpha^*|}{Re_p} \right)^{1/2} - 0.875\alpha^* + 2\Omega^*. \tag{3.5}$$

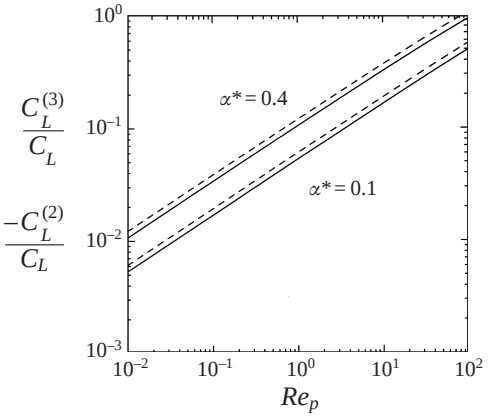

FIGURE 7. Contributions of the second and third terms, $C_L^{(2)}$ and $C_L^{(3)}$, in (3.5) to the total lift coefficient C_L for $\Omega^* = 0.5\alpha^*$: ——, $C_L^{(2)}$; – – –, $C_L^{(3)}$.

The contributions of the second and third terms on the right-hand side of (3.5) to the total lift coefficient, $C_L{}^{(2)}$ and $C_L{}^{(3)}$, are less than 10% for $Re_p < 1$ as shown in figure 7. Here, the rotational angular speed Ω^* was set to $0.5\alpha^*$ on the assumption that the rotation of a freely rotating sphere is induced by the fluid shear. Therefore, the second and third terms are not so important for $Re_p < 1$. McLaughlin (1991) also extended the Saffman's analysis for smaller ϵ in (3.4), and Mei (1992) obtained

$$\frac{C_L}{C_{L,Sa}} = 0.443J, \tag{3.6}$$

from the McLaughlin's (1991) results. Here the subscript Sa means the value given by Saffman's expression (3.5) neglecting the second and third terms on the right-hand side. The non-dimensional quantity J is given by

$$J = J(\epsilon) \approx 0.6765\{1 + \tanh\,[2.5\log_{10}(\epsilon + 0.191)]\}\{0.667 + \tanh\,[6(\epsilon - 0.32)]\}, \tag{3.7}$$

Equation (3.7) was constructed by Mei (1992) from the results of McLaughlin (1991) for $0.1 \leqslant \epsilon \leqslant 20$. By carefully examining the numerical results of Dandy & Dwyer (1990), Mei (1992) proposed the following formula for the lift coefficient:

$$\frac{C_L}{C_{L,Sa}} = \begin{cases} (1 - 0.3314\alpha^{*1/2})\exp\,(-\frac{1}{10}Re_p) + 0.3314\alpha^{*1/2}, & Re_p \leqslant 40 \\ 0.0524(\alpha^{*1/2}Re_p)^{1/2}, & Re_p > 40. \end{cases} \tag{3.8}$$

Figure 8 shows comparisons of the lift coefficient C_L obtained by the present simulation with the approximate expressions given by Saffman (1965), McLaughlin (1991) and Mei (1992) for a stationary sphere in a linear shear flow with $\alpha^* = 0.1$ and 0.4. To clearly show the difference including the change of the sign of C_L, both logarithmic (*a*) and linear (*b*) graphs are used. For Saffman's expression (3.5), the second and third terms on the right-hand side were neglected here. C_L rapidly decreases with increasing Re_p in the low particle Reynolds number range of $Re_p < 10$. Although the present C_L deviates from the predictions by Saffman (1965) and Mei (1992), it is in good agreement with the predictions by McLaughlin (1991) especially for $Re_p \leqslant 5$. However, in the high particle Reynolds number range, the present C_L shows negative values in contrast with the previous results. The negative values of C_L are magnified in figure 9. C_L becomes negative $Re_p > 60$, and the negative value increases with increasing α^*. In previous studies, the lift force has been considered to act from the

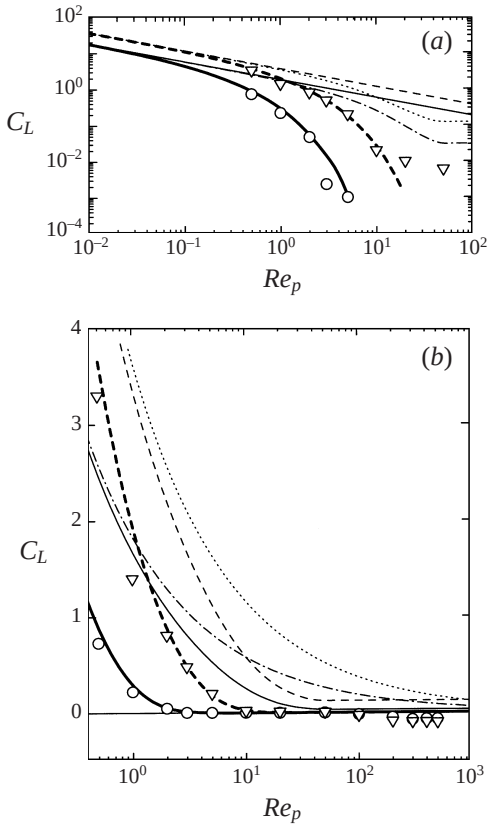

FIGURE 8. Comparisons of lift coefficient C_L for a stationary sphere in a linear shear flow between the present results and the previous results by Saffman (1965), McLaughlin (1991) and Mei (1992): (*a*) logarithmic coordinates; (*b*) linear coordinates: ○, $\alpha^* = 0.1$ (this study); △, $\alpha^* = 0.4$ (this study); ——, $\alpha^* = 0.1$ (Saffman 1965); – – –, $\alpha^* = 0.4$ (Saffman 1965); ▬▬, $\alpha^* = 0.1$ (McLaughlin 1991); ▬ ▬ ▬, $\alpha^* = 0.4$ (McLaughlin 1991); — - — - —, $\alpha^* = 0.1$ (Mei 1992); - - - - -, $\alpha^* = 0.4$ (Mei 1992).

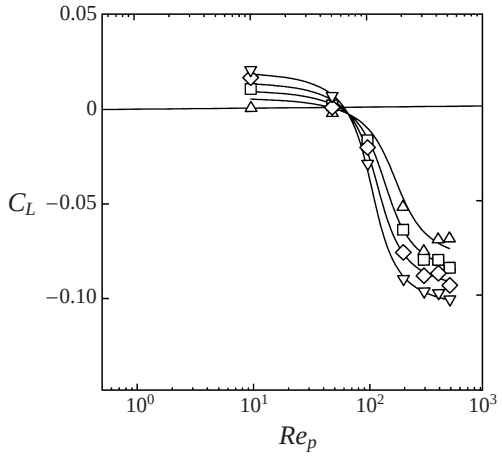

FIGURE 9. Lift coefficient C_L for a stationary sphere in a linear shear flow: △, $\alpha^* = 0.1$; □, $\alpha^* = 0.2$; ◇, $\alpha^* = 0.3$; ▽, $\alpha^* = 0.4$. The distributions of C_L in figure 8 are magnified to show more clearly where the lift force becomes negative.

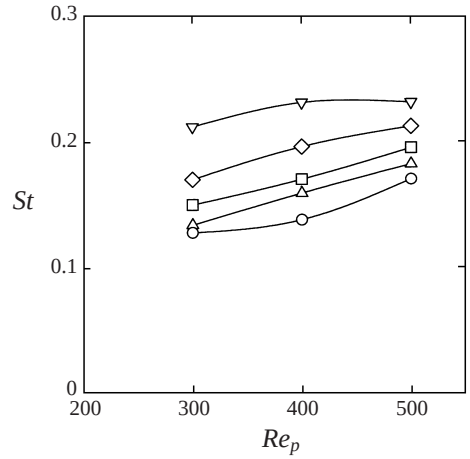

FIGURE 10. Strouhal number for a stationary sphere in a linear shear flow. Symbols as in figures 6 and 9.

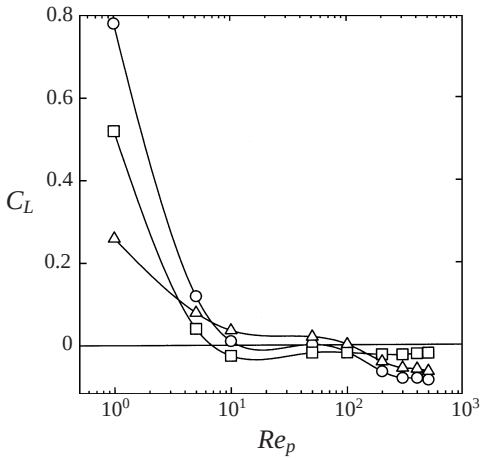

FIGURE 11. Contributions of pressure $C_{L,p}$ and viscous force $C_{L,f}$ acting on a stationary sphere to the total lift coefficient C_L for $\alpha^* = 0.2$: △, $C_{L,p}$; □, $C_{L,f}$; ○, C_L.

lower-fluid-velocity side to the higher-fluid-velocity side ($C_L > 0$). Only Jordan & Fromm (1972) suggested the negative C_L for a cylinder with $Re = 400$ in a linear shear flow by using a two-dimensional numerical simulation. However, they did not give a physical explanation for it.

Figure 10 shows the variation of the Strouhal number St obtained from the time history of C_L with the fluid shear rate α^*. St increases with increasing α^*. This trend was first shown by Sakamoto & Haniu (1995), who thought the increase of St was caused by the increase of the entrainment of vorticity on the high-velocity side. A comparison of figure 5 with figure 3 also suggests that the entrainment of vorticity is promoted by the wakes-unsymmetric with respect to the x-axis.

To investigate the generation mechanism of the negative lift in figures 8 and 9, the contributions of pressure $C_{L,p}$ and viscous force $C_{L,f}$ to the total lift C_L for $\alpha^* = 0.2$ are shown in figure 11. The results show that both coefficients $C_{L,p}$ and $C_{L,f}$ change their signs from positive to negative in the range $1 \leqslant Re_p \leqslant 100$. Figures 12 and 13 show

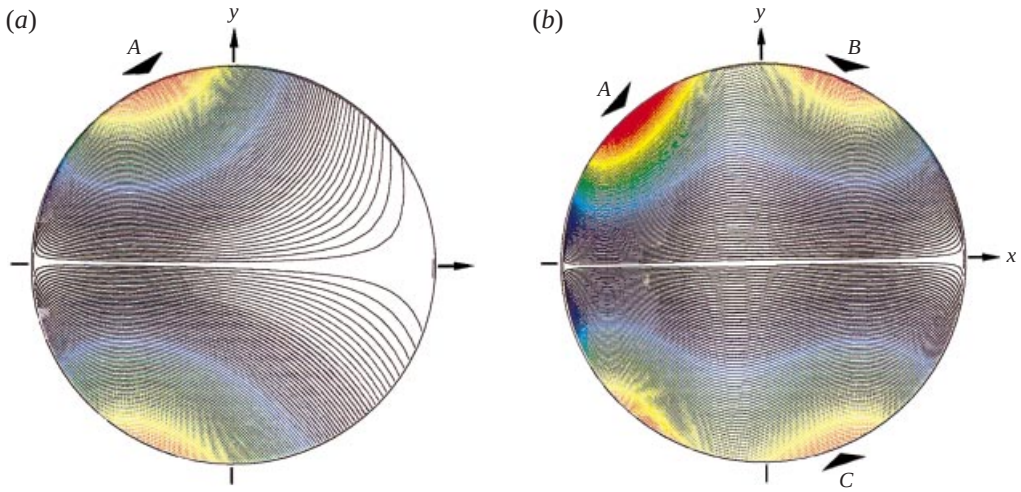

FIGURE 12. Surface contours of the y-component of the instantaneous pressure on the surface of a stationary sphere in a linear shear flow for $\alpha^* = 0.2$: (*a*) $Re_p = 1$; (*b*) $Re_p = 200$. The red and blue lines indicate high and low values of the pressure lift contribution.

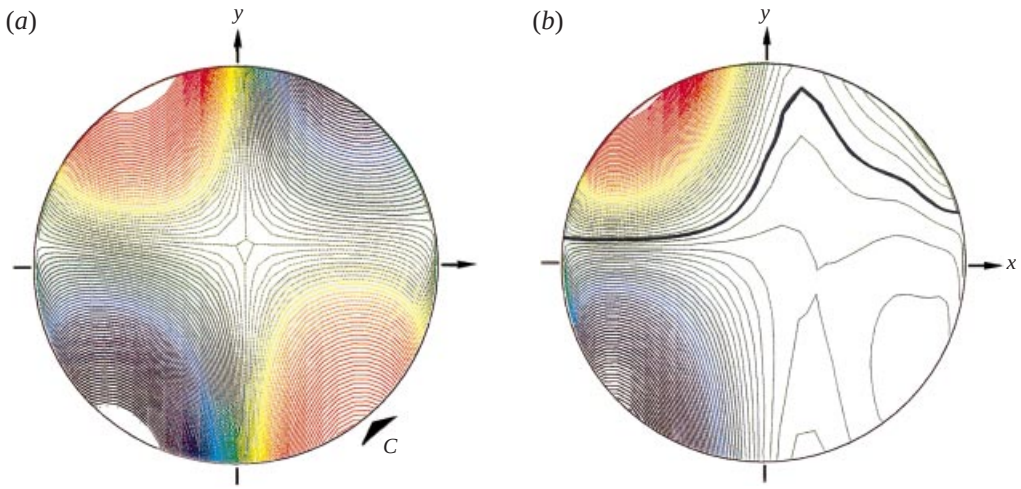

FIGURE 13. Surface contours of y-component of instantaneous viscous force on the surface of a stationary sphere in a linear shear flow for $\alpha^* = 0.2$: (*a*) $Re_p = 1$; (*b*) $Re_p = 200$. The red and blue lines indicate positive and negative values of the viscous lift contribution. The thick line in (*b*) shows the zero value of the instantaneous viscous force.

the surface contours of the y-component of the instantaneous pressure and viscous force on the sphere for $Re_p = 1$ and 200. The variations of $C_{L,p}$ and $C_{L,f}$ with Re_p in figure 11 can be explained by using figures 12 and 13, as follows. Strong downward pressure appears on the front side of the sphere for both $Re_p = 1$ and 200, as indicated by arrows A in figures 12(*a*) and 12(*b*). However, the integrated value of the pressure over the whole surface $C_{L,p}$ becomes positive for the low particle Reynolds number of $Re_p = 1$, since the upward pressure is widely distributed over the bottom of the sphere (figure 12*a*). For the high particle Reynolds number of $Re_p = 200$, pressure also acts strongly on both the upper and lower parts of the rear side of the sphere (see arrows

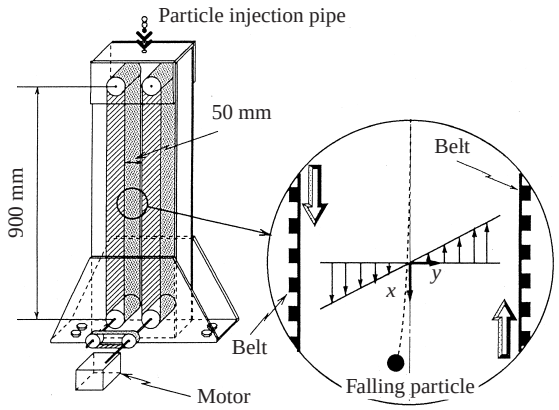

FIGURE 14. Sketch of the experimental apparatus.

B and C in figure 12b). The values of the pressure on the upper and lower parts are roughly comparable, and therefore the strong downward pressure on the front side of the sphere (arrow A) changes the sign of $C_{L,p}$ to negative. The pressure acting on the two places on the rear side of the sphere is attributed to the flow separation behind the sphere. In fact, the flow separation appears at the two places on the rear side of the sphere (see figure 3a). On the other hand, the integrated value of the viscous force over the whole surface $C_{L,f}$ shows positive value for $Re_p = 1$ because the strong upward viscous force is widely distributed over the lower part of the rear side (arrow C in figure 13a), compared with the strong downward viscous force on the upper part. For $Re_p = 200$, the downward viscous force is widely distributed over the surface of the sphere as shown in figure 12(b), and therefore $C_{L,f}$ for the high particle Reynolds numbers takes negative values. The reason why C_L of Dandy & Dwyer (1990) was very different for high Re_p cannot be clarified here. However, recently, Legendre & Magnaudet (1998) who considered the same problem but for a bubble also doubted the accuracy of the results of Dandy & Dwyer (1990). Actually, the present variations of $C_{L,p}$ and $C_{L,f}$ with Re_p (see figure 11) show very similar trends to those of Legendre & Magnaudet (1998) (the contribution of $C_{L,f}$ to C_L decreases with increasing Re_p, and $C_{L,f}$ becomes negative for high Re_p) but not to those of Dandy & Dwyer (1990) ($C_{L,f}$ has a positive value and represents the major contribution to C_L whatever Re_p), despite the difference between a solid particle and a bubble.

3.2. *Experimental verification of negative lift coefficient*

To verify the predictions of the negative lift coefficient experimentally, particle motion was observed in a linear shear flow produced between two belts moving in opposite directions. The apparatus used here was similar to those of Graham & Bird (1984), Kariyasaki (1987) and Cherukat, McLaughlin & Graham (1994) (figure 14). In order to increase the particle Reynolds number and to minimize the turbulence fluctuations in the flow, we dropped an iron particle with diameter of $2a$ (= 2.4, 3.2 or 4.0 mm) and the density of $\rho_p = 7980$ kg m^{-3} into a solution of glycerin and water with kinematic viscosity $\nu_f = 8.96 \times 10^{-6}$ m^2 s^{-1}. Instantaneous vertical (x) and spanwise (y) velocities in the linear shear flow between the two belts were simultaneously measured using a two-colour laser-Doppler velocimeter (DANTEC 55X). The belt speed was carefully adjusted to get adequate values of Re_p and α^* and very low turbulence levels. The measured values of the time-averaged vertical velocity $\overline{U_f}$ [m s^{-1}] with y [m] were

$2a$ (mm)	Re_p	α^*	R^-
2.4	98.8	0.0064	0.535
3.2	167.1	0.0068	0.660
4.0	276.1	0.0064	0.765

TABLE 1. Experimental conditions and the ratio of the number of particles falling in the negative y-direction to the total number of sampled particles.

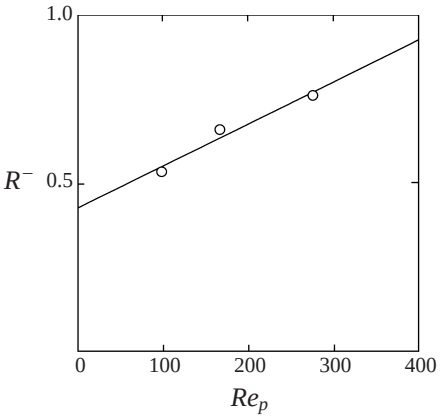

FIGURE 15. The relation between the ratio R^- of the number of the particles falling towards the left-hand side of $y < 0$ to the total number of sampled particles and the particle Reynolds number Re_p in a linear shear flow.

well approximated in the region $-0.35 \leqslant x \leqslant 0.35$ [m] and $-0.02 \leqslant y \leqslant 0.02$ [m] by

$$\overline{U_f} = 1.96y. \tag{3.9}$$

Here the origin $x = 0$ and $y = 0$ corresponded to the center of the apparatus (see figure 14). It was also found that the vertical and spanwise velocity fluctuations in the flow were negligibly small in the region $-0.35 \leqslant x \leqslant 0.35$ [m] and $-0.02 \leqslant y \leqslant 0.02$ [m]. The iron particle was dropped into the linear shear flow field from a particle injection pipe attached on the centre ($y = 0$) of the roof of the apparatus. The trajectory of the particle was recorded at intervals of 0.005 s in the high-speed video system (NAC HSV-400). The rotation rate of the falling particle was also measured by painting half of the white particle black, but it was negligibly small in the weakly sheared flow. Therefore we could neglect the effect of particle rotation on the lift force in this experiment. The measurements were conducted for 200 particles each size (totally 600 particles). For each size, we counted the number of particles falling to the right-hand side (the lower-fluid-velocity side) or to the left-hand side (the higher-fluid-velocity side) in the linear shear flow (see figure 14).

The particle Reynolds number, Re_p, dimensionless fluid shear rate, α^* ($= (a/\overline{U_{rc}})(\partial\overline{U_r}/\partial y)$), and the ratio of the number of the particles falling towards the left-hand side (in the negative y-direction) to the total number of sampled particles, R^-, are listed in table 1. Here, $\overline{U_r}$ ($=| \overline{U_f} - U_p |$) is the difference between the falling velocity of the particle U_p and the vertical velocity of the liquid $\overline{U_f}$. $\overline{U_{rc}}$ is the relative velocity $\overline{U_r}$ of the centre of the particle and it was almost equal to U_p near $y = 0$. Figure 15 shows the correlation between R^- and Re_p. Although the values of α^* were smaller

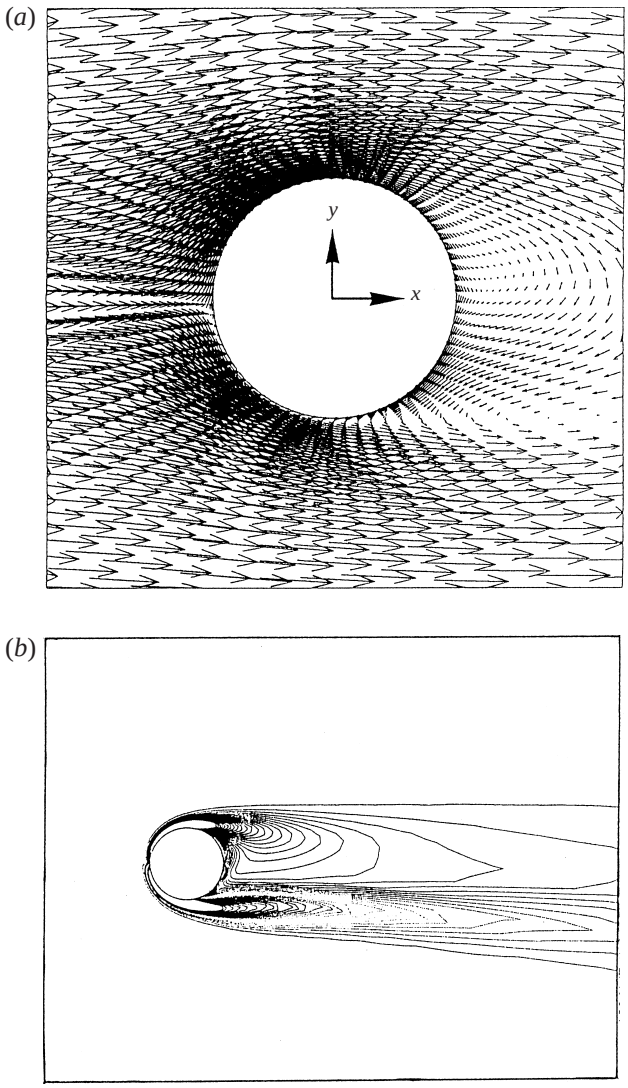

FIGURE 16. Velocity and vorticity fields around a rotating sphere in a uniform unsheared flow on the centreplane ($z = 0$) for $Re_p = 200$ and $\Omega^* = 0.16$: (*a*) velocity field; (*b*) vorticity field.

than the values used for the present simulation, it is clearly seen that R^- increases with increasing Re_p and almost 80% of the 200 particles fall towards the left-hand side for $Re_p = 276.1$. This suggests that the lift force acts towards the lower-fluid-velocity side from the higher-fluid-velocity side for high particle Reynolds numbers. The direction of particle movement is exactly opposite to Saffman's (1965) expression, but it agrees well with the present numerical results shown in figure 9.

3.3. *Drag and lift on a rotating sphere*

To clarify the effects of the rotation of the sphere on the drag and lift forces, computations were conducted in a uniform unsheared flow around a rotating sphere for $1 \leqslant Re_p \leqslant 500$, $\alpha^* = 0$ and $0 \leqslant \Omega^* \leqslant 0.25$. Figure 16 shows the velocity and vorticity fields for this case ($Re_p = 200$, $\Omega^* = 0.16$) on the centreplane ($z = 0$).

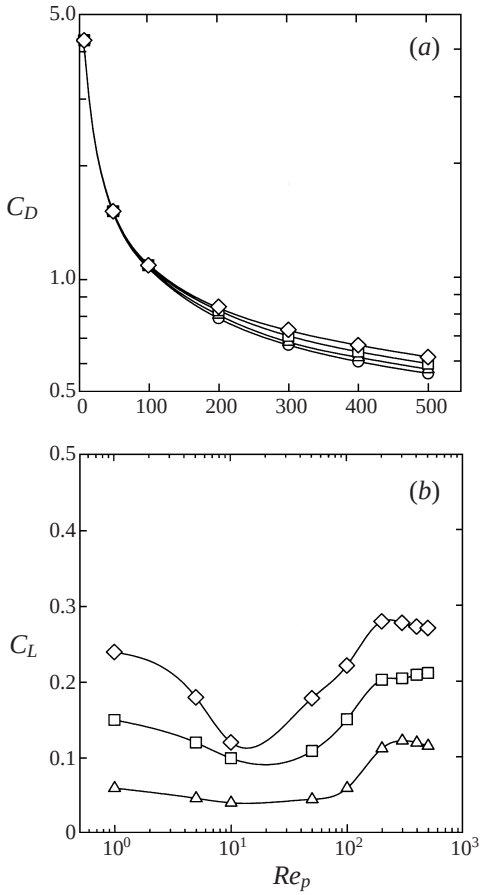

FIGURE 17. Coefficients of drag and lift forces acting on a rotating sphere in a uniform unsheared flow: (*a*) drag coefficient C_D; (*b*) lift coefficient C_L; ○, $\Omega^* = 0$; △, $\Omega^* = 0.063$; □, $\Omega^* = 0.16$; ◇, $\Omega^* = 0.25$.

Comparison of these fields with figure 3 shows that the rotation acts to shift the points of flow separation downstream on the upper side and upstream on the lower side. Figures 17(*a*) and 17(*b*) show the variations of the drag coefficient C_D and lift coefficient C_L with the rotational angular speed of the sphere Ω^* and the particle Reynolds number Re_p. Figure 17(*a*) shows the similar trend of C_D with Ω^* to that of C_D with α^* in figure 6: C_D increases with increasing Ω^*. The difference in C_D between $\Omega^* = 0$ and $\Omega^* = 0.25$ reaches about 10% at $Re_p = 500$. On the other hand, C_L does not change its sign with increasing Re_p in contrast to a stationary sphere in a linear shear flow, and it tends to approach a constant value for $Re_p \geqslant 200$ for a fixed rotational speed. It is also found that the asymptotic value increases with increasing Ω^*. The measurements of C_L by Tsuji *et al.* (1985) ranged from 0.05 to 0.3 for $550 \leqslant Re_p \leqslant 1600$ and $0.1 \leqslant \Omega^* \leqslant 0.5$. The measured values are close to the present asymptotic values for large Re_p in figure 17(*b*), whereas the values of $2\Omega^*$ by Saffman's expression (3.5) were larger than the asymptotic values. The reason why C_L is always positive for a rotating sphere is that the upward pressure acts at the bottom of the sphere as indicated by arrow *D* in figure 18(*a*). That is, the strong pressure $C_{L,p}$ contributes to the total lift C_L as shown in figure 19. Figure 19 also shows that

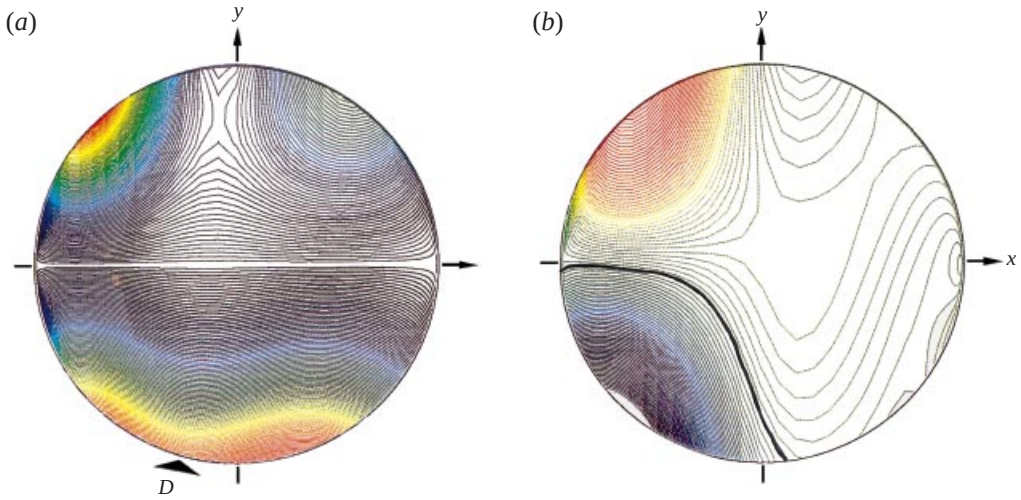

FIGURE 18. Surface contours of the y-component of instantaneous pressure and viscous forces acting on a rotating sphere in a uniform unsheared flow for $Re_p = 200$ and $\Omega^* = 0.16$: (*a*) pressure; (*b*) viscous force. The red and blue lines indicate high and low values of the pressure lift contribution in (*a*), and positive and negative values of the viscous lift contribution in (*b*), respectively. The thick line in (*b*) shows the zero value of the instantaneous viscous force.

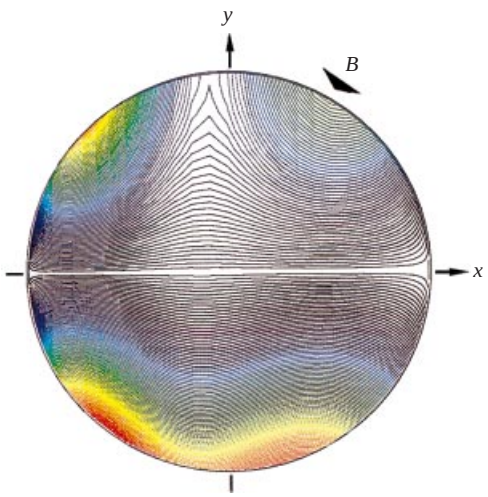

FIGURE 22. Surface contours of the y-component of the instantaneous pressure on a rotating sphere in a linear shear flow for $Re_p = 200$, $\alpha^* = 0.2$ and $\Omega^* = 0.16$. The red and blue lines indicate high and low values of the pressure lift contribution.

the lift coefficient due to the viscous force $C_{L,f}$ is always positive. The positive value of $C_{L,f}$ can be understood from the countours of the instantaneous viscous force in figure 18(*b*). The contour for zero viscous force shifts downward and therefore the positive viscous force widely distributed on the surface of the sphere generates the upward lift.

Figure 20 shows the variation of the Strouhal number St with Ω^*. The trend of St with Ω^* is similar to that of St with α^*: St increases with increasing Ω^*. As the three-dimensional velocity and vorticity fields near the shear layer were not analysed

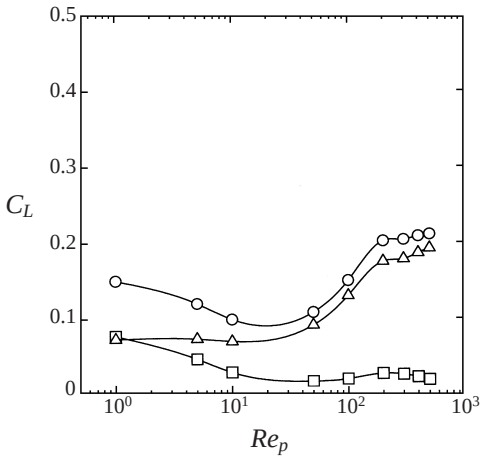

FIGURE 19. Contributions of pressure $C_{L,p}$ and viscous force $C_{L,f}$ acting on a rotating sphere to the total lift coefficient C_L for $\Omega^* = 0.16$: △, $C_{L,p}$; □, $C_{L,f}$; ○, C_L.

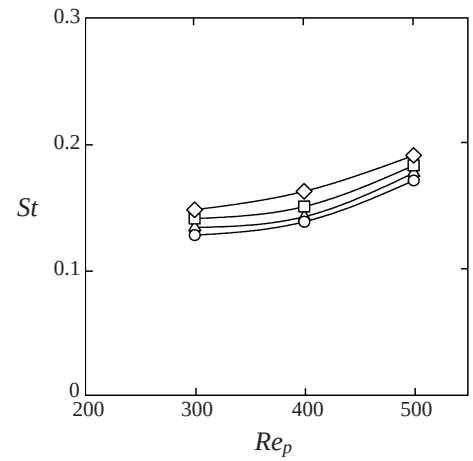

FIGURE 20. Strouhal number for a rotating sphere in a uniform unsheared flow. Symbols as in figure 17.

here, the reason for the increase of St cannot be clarified. However, the explanation of the increase of St with α^* leads us to conclude that the increase of St is caused by the increase of the entrainment of fluid breaking vorticity away from the shear layer on the bottom of the sphere.

It is of great interest to investigate whether the drag and lift forces acting on a rotating sphere in a linear shear flow can be estimated from the drag and lift forces both on a stationary sphere in a linear shear flow with the same shear rate and on a rotating sphere with the same rotational speed in a uniform unsheared flow. If the drag and lift forces can be estimated in this way, the effects of the fluid shear and rotation can be treated independently. The computations for a linear shear flow around a rotating sphere were carried out for $1 \leqslant Re_p \leqslant 500$, $0 \leqslant \alpha^* \leqslant 0.4$ and $0 \leqslant \Omega^* \leqslant 0.25$. Figures 21($a$) and 21($b$) show the variation of the lift coefficient with the dimensionless rotational speed Ω^* for $Re_p = 1$ and 200. The solid lines indicate the lift coefficient C_L ($= C_L^{\alpha+\Omega}$) for a rotating sphere in a linear shear flow, and the

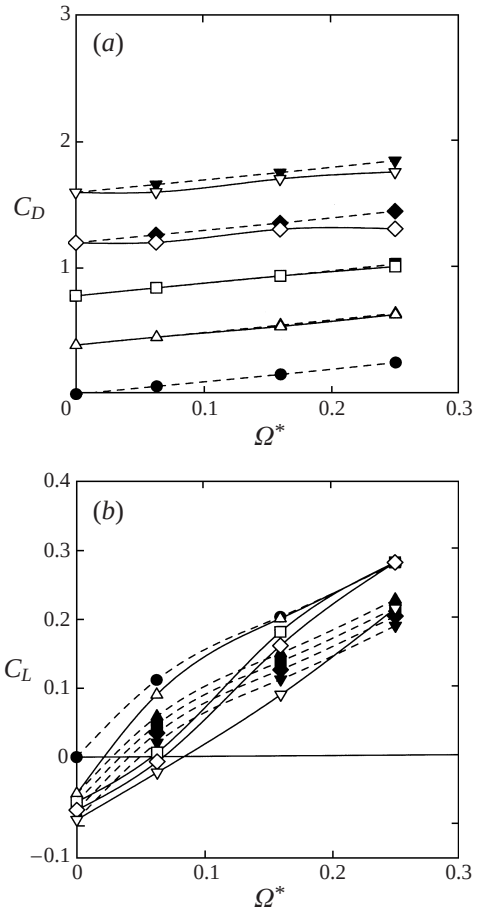

FIGURE 21. Comparisons of lift coefficient C_L for a rotating sphere in a linear shear flow (open symbols) with the sum of the lift coefficients for a stationary sphere in a linear shear flow with the same α^* and for a rotating sphere with the same Ω^* in a uniform unsheared flow (solid symbols): (*a*) $Re_p = 1$; (*b*) $Re_p = 200$. Symbols as in figures 6 and 9.

dashed lines show the sum of the lift coefficient C_L^{α} for a stationary sphere in a linear shear flow with the same α^* and the lift coefficient C_L^{Ω} for a rotating sphere with the same Ω^* in a uniform unsheared flow. The values of C_L ($= C_L^{\alpha+\Omega}$) are close to those of $C_L^{\alpha}+C_L^{\Omega}$ for $Re_p = 1$, whereas for $Re_p = 200$, they are different. The variation of C_L with Ω^* is very complicated for high Re_p. This means that the effects of the fluid shear and rotation on a rotating sphere in a shear flow cannot be independently treated for high particle Reynolds numbers. Although comparisons of the drag coefficients C_D are not shown here, the behaviour of C_D was the same as in the case of C_L in figure 21. Of course, in the case of C_D, the deviations for a stationary sphere in a uniform unsheared flow were considered. Furthermore, for the low particle Reynolds numbers of $Re_p < 1$, the deviations were almost zero. This means that the effects of the fluid shear and rotation on C_D for a rotating sphere in a linear shear flow are negligibly small for $Re_p < 1$, and therefore C_D can be estimated by the expression of Morsi & Alexander (1972). The reason why $C_D^{\alpha+\Omega}$ or $C_L^{\alpha+\Omega}$ cannot be estimated by using C_D^{α} and C_D^{Ω} or C_L^{α} and C_L^{Ω} for high particle Reynolds numbers and why they have complicated variations for Ω^* is that the flow separation is strongly affected by both

Re_p	K_0	K_1	K_2	K_3	K_4	K_5	K_6
1	0	-1.804×10^{-15}	-1.726×10^{-18}	3.296×10^{-18}	-1.010×10^{-14}	-1.114×10^{-17}	4.286×10^{-17}
5	1.417×10^{-2}	1.445×10^{-3}	1.773×10^{-3}	-3.404×10^{-3}	6.289×10^{-2}	5.676×10^{-2}	-1.407×10^{-1}
10	2.298×10^{-2}	2.237×10^{-3}	5.706×10^{-3}	-6.871×10^{-3}	1.150×10^{-1}	-2.343×10^{-1}	4.205×10^{-1}
50	6.473×10^{-2}	6.634×10^{-3}	-6.437×10^{-3}	1.154×10^{-2}	2.981×10^{-1}	2.518×10^{-2}	-2.655×10^{-1}
100	6.523×10^{-2}	9.248×10^{-3}	3.358×10^{-3}	-4.478×10^{-3}	4.177×10^{-1}	-1.238×10^{-1}	2.676×10^{-1}
200	1.216×10^{-1}	1.125×10^{-1}	-4.687	6.343	4.599	7.590×10^{1}	-1.641×10^{2}
300	1.344×10^{-1}	1.227×10^{-1}	-5.416	7.347	9.776	7.196×10^{1}	-2.519×10^{2}
400	2.101×10^{-1}	1.336×10^{-1}	-5.885	7.875	1.017×10^{1}	5.217×10^{1}	-1.921×10^{2}
500	2.440×10^{-1}	1.285×10^{-1}	-6.303	8.509	9.826	4.141×10^{1}	-1.622×10^{2}

TABLE 2. Constants in (3.10).

Re_p	K_0	K_1	K_2	K_3	K_4	K_5
1	4.815×10^{-1}	3.578	9.741×10^{-1}	7.523	-3.252×10^{1}	1.419×10^{4}
5	-7.830×10^{-1}	1.746	7.283×10^{-1}	3.975	-1.482×10^{1}	6.710×10^{3}
10	-9.408×10^{-2}	1.886×10^{-1}	6.801×10^{-1}	8.419×10^{-2}	-7.252×10^{-1}	1.161×10^{3}
50	-1.141×10^{-1}	1.533×10^{-1}	7.108×10^{-1}	2.455×10^{-1}	-1.034	3.668×10^{2}
100	-1.823×10^{-1}	1.242×10^{-1}	9.261×10^{-1}	4.736×10^{-1}	-1.592	5.660×10^{2}
200	-4.269×10^{-1}	2.455×10^{-1}	1.244	1.002	-1.843	-8.679×10^{2}
300	-1.112	1.101	1.269	2.386	-9.355	1.938×10^{3}
400	-9.983×10^{-1}	9.250×10^{-1}	1.275	1.470	-5.201	3.065×10^{2}
500	-6.926×10^{-1}	5.305×10^{-1}	1.239	1.389	-4.556	5.207×10^{2}

TABLE 3. Constants in (3.11).

shear and rotation. In fact, as shown in figure 22 (see page 199), the pressure acting on the upper rear part indicated by the arrow B for a rotating sphere in a linear shear flow is much weaker than that for a stationary sphere in a linear shear flow, and the maximum pressure point on the upper rear part slightly shifts downstream compared to the point indicated by the arrow B in figure 12(b).

Because of the complicated variations of the drag and lift coefficients with the shear rate α^* and rotational speed Ω^*, it is not easy to give C_D and C_L for a rotating sphere in a linear shear flow for arbitrary α^* and Ω^* especially for high particle Reynolds numbers. However, to simulate rotating particle motion in an arbitrary shear flow, approximate expressions for C_D and C_L for arbitrary α^*, Ω^* and Re_p will be required. Therefore, by using the predictions of $C_D(Re_p, \alpha^*, \Omega^*)$ and $C_L(Re_p, \alpha^*, \Omega^*)$ for $0 \leqslant \alpha^* \leqslant 0.4$ and $0 \leqslant \Omega^* \leqslant 0.25$, the following expressions were proposed for nine values of $Re_p = 1$, 5, 10, 50, 100, 200, 300, 400 and 500:

$$C_D(Re_p, \alpha^*, \Omega^*) = C_D(Re_p, \alpha^* = 0, \Omega^* = 0) \times [1 + K_0\alpha^* + (K_1 + K_2\alpha^{*1.5} + K_3\alpha^{*2.0})\Omega^{*0.5} + (K_4 + K_5\alpha^* + K_6\alpha^{*2.0})\Omega^{*4.0}], \quad (3.10)$$

$$C_L(Re_p, \alpha^*, \Omega^*) = K_0\alpha^{*0.9} + K_1\alpha^{*1.1} + (K_2 + K_3\alpha^* + K_4\alpha^{*2.0} + K_5\alpha^{*9.5})\Omega^*, \quad (3.11)$$

where $C_D(Re_p, \alpha^* = 0, \Omega^* = 0)$ is the drag coefficient for a stationary sphere in a uniform unsheared flow. The values of K_0–K_6 in (3.10) and (3.11) are listed in tables 2 and 3. By interpolating the values of C_D and C_L from (3.10) and (3.11) for nine values of Re_p, C_D and C_L were calculated for arbitrary particle Reynolds numbers ($1 \leqslant Re_p \leqslant 500$). Figures 23 and 24 compare the interpolated values of C_D and C_L from (3.10) and (3.11) with the numerical predictions. The value of $C_D(Re_p, \alpha^* = 0, \Omega^* = 0)$ is given Morsi & Alexander (1972) here. Both interpolated and simulated values well agree. The good agreement suggests that C_D and C_L for a rotating sphere in a linear shear flow for $Re_p \leqslant 500$, $0 \leqslant \alpha^* \leqslant 0.4$ and $0 \leqslant \Omega^* \leqslant 0.25$ can be well estimated by using (3.10) and (3.11).

4. Conclusions

The numerical simulation was done for a linear shear flow around a rotating sphere over a wide range of the particle Reynolds number ($1 \leqslant Re_p \leqslant 500$). The main results from this study can be summarized as follows.

(i) Both the fluid shear rate and the rotational angular speed of a sphere promote the drag coefficient. Their effects are enhanced with increasing the particle Reynolds number.

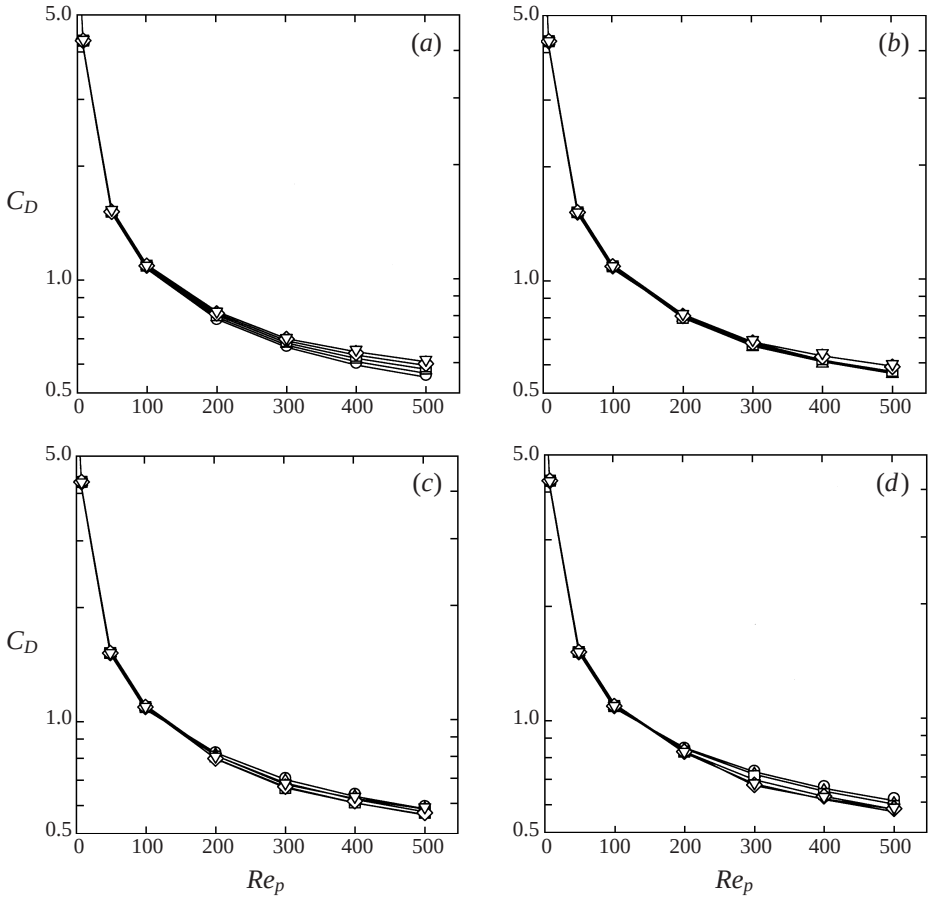

FIGURE 23. Comparisons of the drag coefficient C_D obtained by interpolating the values from the approximate expressions in (3.10) for arbitrary α^* and Ω^* with that obtained by the three-dimensional numerical simulations: (*a*) $\Omega^* = 0$; (*b*) $\Omega^* = 0.063$; (*c*) $\Omega^* = 0.16$; (*d*) $\Omega^* = 0.25$. The lines for several α^* show the interpolated results from (3.10) and the symbols show the simulated values. Symbols as in figures 6 and 9.

(ii) The lift coefficient for a stationary sphere in a linear shear flow rapidly decreases with increasing particle Reynolds number, and it has negative values in the range $Re_p > 60$. This means that the lift force acts from the higher-fluid-velocity side to the lower-fluid-velocity side for high particle Reynolds numbers. The negative lift is attributed to the flow separation behind the sphere.

(iii) The lift coefficient for a rotating sphere in a uniform unsheared flow tends to approach to a constant value for high particle Reynolds numbers $Re_p > 200$. The asymptotic value increases with increasing the rotational speed.

(iv) Equations (3.10) and (3.11) estimate well the drag and lift coefficients for a rotating sphere in a linear shear flow with $1 \leqslant Re_p \leqslant 500$.

(v) The Strouhal number of the vortex shedding from a sphere increases with increasing both the fluid shear rate and the rotational angular speed of a sphere.

The authors thank Dr H. Hanazaki of Tohoku University for his kind suggestion in remaking his original program code for this study, and they also thank K. Fujikawa, K. Nakamura, T. Yamashita and Y. Shibata for their great help in conducting

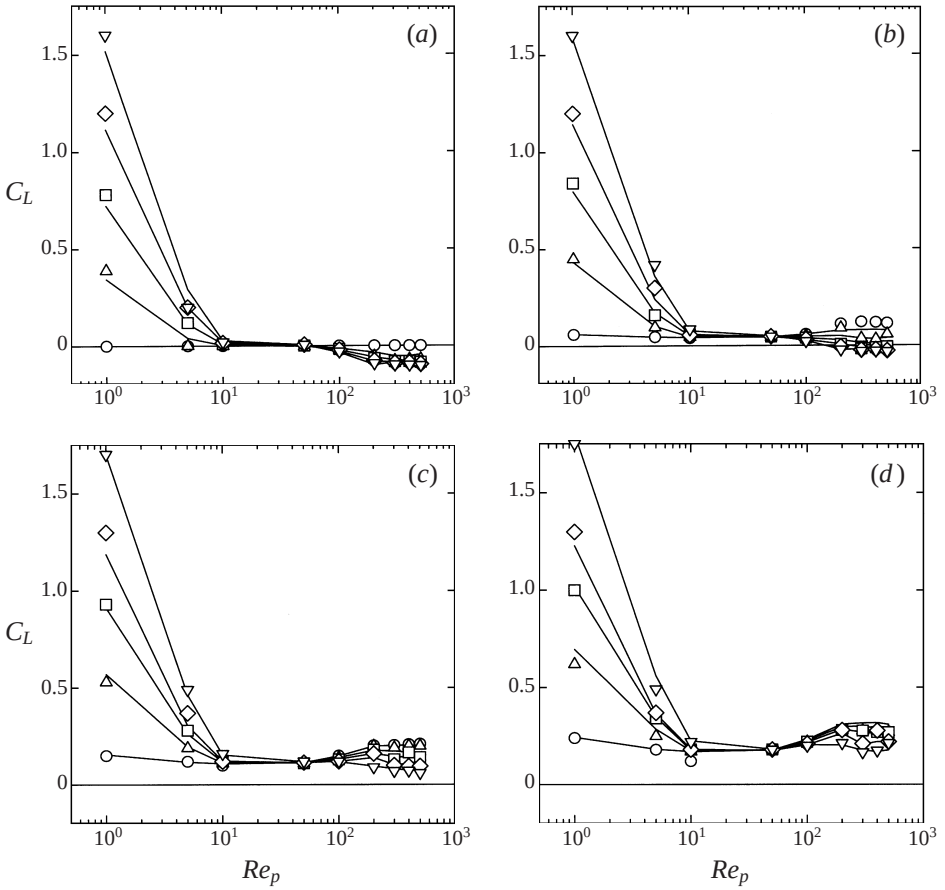

FIGURE 24. Comparisons of the lift coefficient C_L obtained by interpolating the values from the approximate expression in (3.11) with that obtained by the three-dimensional numerical simulations: (*a*) $\Omega^* = 0$; (*b*) $\Omega^* = 0.063$; (*c*) $\Omega^* = 0.16$; (*d*) $\Omega^* = 0.25$. The lines for several α^* show the interpolated values from (3.11) and the symbols show the simulated values. Symbols as in figures 6 and 9.

experiments and numerical simulations. This work was supported by the Japan Ministry of Education, Science and Culture through Grants-in-Aid (Nos. 072274 and 09450079). The computations were conducted by the super computer of the Center for the Global Environmental Research, National Institute for Environmental Studies, Environment Agency of Japan.

REFERENCES

BARKLA, H. M. & AUCHTERLONIE, L. J. 1971 The magnus or robins effect on rotating sphere. *J. Fluid Mech.* **47**, 437–448.

CHERUKAT, P., MCLAUGHLIN, J. B. & GRAHAM, A. L. 1994 The inertial lift on a rigid sphere in a linear shear flow field. *Intl J. Multiphase Flow* **20**, 339–354.

DANDY, D. S. & DWYER, H. A. 1990 A sphere in shear flow at finite Reynolds number : effect of shear on particle lift, drag, and heat transfer. *J. Fluid Mech.* **216**, 381–410.

GRAHAM, A. L. & BIRD, R. B. 1984 Particle clusters in concentrated suspensions. 1. Experimental observations of particle clusters. *Ind. Engng Chem. Fundam.* **23**, 406–410.

HALL, D. 1988 Measurements of the mean force on a particle near a boundary in turbulent flow. *J. Fluid Mech.* **187**, 451–466.

Hanazaki, H. 1988 A numerical study of three-dimensional stratified flow past a sphere. *J. Fluid Mech.* **192**, 393-419.

Harper, E. Y. & Chang, I. D. 1968 Maximum dissipation resulting from lift in a slow viscous shear flow. *J. Fluid Mech.* **33**, 209–225.

Jordan, S. K. & Fromm, J. E. 1972 Laminar flow past a circle in a shear flow. *Phys. Fluids* A **16**, 972–976.

Kariyasaki, A. 1987 Behavior of a single gas bubble in a liquid flow with a linear velocity profile. In *Proc. 1987 ASME-JSME Thermal Engineering Joint Conference*. Vol. 5, 261–267.

Kawamura, T. & Kuwahara, K. 1984 Computation of high Reynolds number flow around a circular cylinder with surface roughness. *AIAA Paper* 84-0340.

Legendre, D. & Magnaudet, J. 1998 The lift force on a spherical bubble in a viscous linear shear flow. *J. Fluid Mech.* **368**, 81–126.

McLaughlin, J. B. 1991 Inertial migration of a small sphere in linear shear flows. *J. Fluid Mech.* **224**, 261–274.

Mei, R. 1992 An approximate expression for the shear lift force on a spherical particle at finite Reynolds number. *Intl J. Multiphase Flow* **18**, 145–147.

Mollinger, A. M. & Nieuwstadt, F. T. M. 1996 Measurement of the lift force on a particle fixed to the wall in the viscous sublayer of a fully developed turbulent boundary layer. *J. Fluid Mech.* **316**, 285–306.

Morsi, S. A. & Alexander, A. J. 1972 An investigation of particle trajectories in two-phase systems. *J. Fluid Mech.* **55**, 193–208.

Rabindra, D. M. 1985 Aerodynamics of sports balls. *Ann. Rev. Fluid Mech.* **17**, 151–189.

Rubinow, S. I. & Keller, J. B. 1961 The transverse force on a spinning sphere moving in a viscous fluid. *J. Fluid Mech.* **11**, 447–459.

Saffman, P. G. 1965 The lift on a small sphere in a slow shear flow. *J. Fluid Mech.* **22**, 385-400 (and Corrigendum **31**, 1968, 624).

Sakamoto, H. & Haniu, H. 1995 The formation mechanism and shedding frequency of vortices from a sphere in uniform shear flow. *J. Fluid Mech.* **287**, 151–171.

Salem, M. B. & Oesterle, B. 1995 A numerical investigation of the force and the torque on a spinning spherical particle suspended in a linear shear flow. In *Proc. 2nd Intl Conf on Multiphase Flow* (ed. A. Serizawa, T. Fukano & J. Bataille), Vol. 2, pp. PD3-19–PD3-25. Kyoto, Japan.

Thames, F. C., Thompson, J. F., Mastin, C. W. & Walker, R. L. 1977 Numerical solutions for viscous and potential flow about arbitrary two-dimensional bodies using body-fitted coordinate systems. *J. Comput Phys.* **24**, 245–273.

Tsuji, Y., Morikawa, Y. & Mizuno, O. 1985 Experimental measurement of the magnus force on a rotating sphere at low Reynolds numbers. *Trans. ASME* **107** no. 4, 484–488.